International Journal of Biology and Life Sciences
ISSN: 2957-9511 | Vol. 9, No. 3, 2025

Circular RNA hsa_circ_0006421 inhibits hepatocellular carcinoma by acting as a ceRNA targeting miR-134-5p/CELF2 pathway

Lv Zhou [1, 2], Junhao Shi [2], Junxia Pu [2, 3], Xiaohao Chen [3] and Yibin Deng [2, 3, 4, *]

[1] Central People's Hospital of Zhanjiang, Zhanjiang, Guangdong, China
[2] Youjiang Medical University for Nationalities, Baise, Guangxi, China
[3] The Affiliated Hospital of Youjiang Medical University for Nationalities, Baise, Guangxi, China
[4] Baise Key Laboratory of Clinical Molecular Diagnosis, Research and Development for High Incidence Diseases, Baise, Guangxi, China

*** Corresponding author:** Yibin Deng (Email: 1123049646@qq.com)

Abstract: Background: Hepatocellular carcinoma (HCC), ranking as the sixth most prevalent malignancy globally, exhibits substantial clinical burden. Emerging evidence underscores the critical involvement of circular RNAs (circRNAs) in the pathogenesis of various malignancies. While hsa_circ_0006421 has been implicated in gastric cancer progression, its functional significance in HCC remains unexplored. This study investigates the mechanistic role of hsa_circ_0006421 in HCC pathogenesis. Methods: Differentially expressed circRNAs in HCC tissues were identified through integrated bioinformatics analysis of the GSE97332 dataset and high-throughput sequencing of clinical specimens. Functional characterization of hsa_circ_0006421 was performed using in vitro cellular models (HepG2, MHCC97H) and xenograft experiments. Molecular interactions were validated via qRT-PCR, Western blot, and dual-luciferase reporter assays. Results: Clinical analyses revealed significant downregulation of hsa_circ_0006421 in HCC tissues, particularly in patients with cirrhosis history. Functional studies demonstrated that hsa_circ_0006421 overexpression suppressed HCC proliferation, migration, and invasion. Mechanistically, hsa_circ_0006421 functioned as a competitive endogenous RNA by sequestering miR-134-5p, thereby alleviating its inhibitory effect on CELF2 expression. A negative regulatory relationship between miR-134-5p and CELF2 was established, with hsa_circ_0006421 restoration significantly upregulating CELF2 protein levels in HCC cells. Conclusion: Our findings elucidate a novel hsa_circ_0006421/miR-134-5p/CELF2 regulatory axis that suppresses HCC progression, providing potential therapeutic targets for HCC management.

Keywords: Hepatocellular Carcinoma; CELF2; miR-134-5p; hsa_circ_0006421.

1. Introduction

As evidenced by 2020 GLOBOCAN statistics, hepatocellular carcinoma (HCC) emerges as the sixth most prevalent neoplasm globally and the third principal contributor to oncological deaths, with its clinical management complicated by a narrow therapeutic arsenal and substantial disease burden. [1-2]. Notably, China bears a disproportionate disease burden, contributing 47.1% of global HCC fatalities and 45.6% of incident cases, underscoring the urgent need for novel biomarkers to enhance early detection and prognostic stratification. Emerging evidence implicates dysregulated non-coding RNAs (ncRNAs) in HCC pathogenesis, positioning these molecules as promising diagnostic and predictive candidates.

Circular RNAs (circRNAs), first identified in eukaryotic systems in 1979, were historically dismissed as splicing artifacts but are now recognized for their enhanced stability conferred by covalently closed structures. Compelling studies reveal aberrant circRNA expression patterns across multiple malignancies, including cervical, breast [9-10], colorectal, and gastric cancers, as well as HCC. High-throughput sequencing of clinical specimens and GSE97332 dataset analysis identified 28 differentially expressed circRNAs in HCC, including hsa_circ_0006421—a molecule previously associated with gastric cancer suppression but mechanistically uncharacterized in hepatic carcinogenesis.

Current paradigms position circRNAs as critical regulators of oncogenic pathways through miRNA sponging or RNA-binding protein interactions [15-16]. Our bioinformatic interrogation (Starbase v3.0) revealed potential tripartite interactions among hsa_circ_0006421, miR-134-5p, and CELF2, suggesting a novel hsa_circ_0006421/miR-134-5p/CELF2 regulatory axis in HCC. This study systematically investigates the tumor-suppressive mechanisms of hsa_circ_0006421, focusing on its ceRNA-mediated regulation of miR-134-5p and downstream CELF2 modulation.

2. Materials and Methods

2.1. Identification of Differentially Expressed CircRNAs

The GSE97332 dataset associated with hepatocellular carcinoma (HCC) was acquired from the Gene Expression Omnibus database (GEO, https://www. ncbi. nlm.nih. gov/geo/). Paired tissue samples comprising five HCC specimens and corresponding adjacent normal tissues were collected from surgical patients at Youjiang Medical University for Nationalities, with all participants providing signed informed consent forms. This research protocol received ethical approval from the institution's Medical Ethics Committee (Approval Number: 2019012601). Clinical specimens were subsequently transported to BGI Genomics Co., Ltd. for comprehensive high-throughput sequencing. Differential expression analysis of circular RNAs (DE-circRNAs) was performed using the limma package in R software, comparing

transcriptional profiles between malignant and paracancerous tissues. Bioinformatics analysis integrating both GEO dataset and sequencing data revealed significant DE-circRNAs through comparative analysis, with subsequent intersection analysis conducted using pheatmap and VennDiagram packages to identify consensus molecular markers.

2.2. Patients and Sample Collection

Thirty-four pairs of fresh hepatocellular carcinoma (HCC) specimens and adjacent non-tumor tissues were collected from surgical resections at the Affiliated Hospital of Youjiang Medical University for Nationalities. This study received ethical approval from the institution's Medical Ethics Committee (Approval No: YYFY-LL-2022-13) prior to sample collection. All participants provided written informed consent, with exclusion criteria applied to patients who had undergone preoperative chemoradiotherapy. Pathological confirmation of HCC diagnosis was obtained for all included cases. Immediately following surgical resection, tissue samples were snap-frozen in liquid nitrogen and maintained at -80°C until subsequent experimental analysis.

2.3. Cell Lines and Cultures

The HepG2 hepatocellular carcinoma cell line and HEK293T human embryonic kidney cells were obtained from the Chinese Academy of Sciences Cell Bank (Beijing), while MHCC97H HCC cells were commercially acquired from Cellcook Biotech (Guangzhou). All cell lines were maintained in high-glucose DMEM medium (Gibco) supplemented with 10% fetal bovine serum (Beyotime) under standard culture conditions (37℃, 5% CO_2, humidified atmosphere). Routine cell authentication and mycoplasma contamination testing were performed to ensure experimental validity.

2.4. Cell Transfection

HepG2 and MHCC97H cell lines were transduced with lentiviral vectors containing shRNA targeting hsa_circ_ 0006 421 (sh-circ) or non-targeting control (sh-NC) at an MOI of 100. Subsequently, lentivirus-stably transformed cells were selected using 4 μg/mL puromycin in complete medium. For ectopic expression of hsa_circ_0006421 (over-circ), the full-length cDNA sequence was synthesized and subcloned into pcDNA3.1 expression vector. All molecular reagents including miR-134-5p mimic, hsa_circ_0006421-specific siRNA (si-circ), shRNA (sh-circ), and corresponding negative controls were procured from GenePharma Co., Ltd. (Suzhou, China) **(Table 1)**. Transfection procedures were performed using Lipofectamine 3000 reagent (Invitrogen, Thermo Fisher Scientific, USA) following manufacturer's protocols.

2.5. Purification of RNA and Subsequent qRT-PCR Assessment

Total RNA from HCC tissues and cultured cells was isolated with TRIzol reagent (Invitrogen) and subsequently converted to complementary DNA (cDNA) using RevertAid Master Mix (ThermoFisher). For miRNA analysis, qRT-PCR was performed using miRNA First Strand cDNA Synthesis kit (Sangon Biotech, China). The synthesized cDNA was evaluated by qRT-PCR using SYBR Green (Hieff®, Shanghai, China). The amplification reaction conditions were as follows: 95°C for 10 s and 60°C for 30 s.Normalization of target gene expression was achieved using U6 and GAPDH as endogenous controls. Detailed primer sequences are provided in **Table 1**.

Table 1. Oligonucleotide specifications for RNA interference agents (siRNA/shRNA), miRNA-134-5p mimics, and validated PCR primer pairs

Name	Sequence (5'-3')
si-circ_0006421:	Sense: 5'AGAGGAGUGGAAGCAGAACTT3' Antisense: 5'GUUCUGCUUCCACUCCUCUTT3'
sh-circ_0006421:	Sense: 5'-CAGAGGAGUGGAAGCAGAATT-3' Antisense：5'-UUCUGCUUCCACUCCUCUGGU-3'
miR-134-5p mimic:	Sense: 5'-UGUGACUGGUUGACCAGAGGGG-3' Antisense: 5'-CCUCUGGUCAACCAGUCACAUU-3'
hsa_circ_0006421:	Forward: 5'-ACTGGCTTCACGTGGATATGG-3' Reverse: 5'-CCAGTTCTGCTTCCACTCCTC-3'
miR-134-5p:	Forward: 5'- CCTCTATTCTGTGACTGGTTGACC -3' Reverse: 5'- TATGGTTTTGACGACTGTGTGAT -3'
CELF2:	Forward: 5'-CTGGCGGGAAACAAACTCTG-3' Reverse: 5'-TCTAAGCCCTTGGCCTCCTC-3'
GAPDH:	Forward: 5'-CAGGAGGCATTGCTGATGAT-3' Reverse: 5'-GAAGGCTGGGGCTCATTT-3'
U6:	Forward:5'-CAGCACATATACTAAAATTGGAACG-3' Reverse: 5'-ACGAATTTGCGTGTCATCC-3'

2.6. Cell Proliferation Assay

HepG2 and MHCC97H hepatocellular carcinoma cells were seeded in 96-well plates at a density of 3×10^3 cells per well. Peripheral wells were filled with phosphate-buffered saline (PBS) to minimize edge effects during incubation. Prior to optical density measurement, 10μL of CCK-8 solution (MedChemExpress, China) was aliquoted into each experimental well. Following a 2-hour incubation period at 37°C with 5% CO_2, the absorbance at 450 nm was quantified using a microplate reader to assess cellular metabolic activity.

2.7. Colony Formation Assay

Stably transfected lentiviral cell lines were seeded at a uniform density of 1.7×10^3 cells/well in 6-well plates. Medium replacement was performed every 3 days using DMEM supplemented with 20% fetal bovine serum (FBS). After 9 days of culture when distinct colonies had formed, the experiment was terminated. Cellular fixation was achieved through 20-minute treatment with 4% paraformaldehyde. Subsequent staining procedures involved 15-minute exposure to crystal violet solution followed by thorough rinsing. The

resulting clones were quantified and statistically evaluated through microscopic examination.

2.8. Cell Migration Assay

Hepatocellular carcinoma cell lines (HepG2 and MHCC97H) were plated in six-well culture dishes and subjected to serum starvation for 24 hours. Following this pretreatment, the cells were maintained under standard culture conditions (37°C, 5% CO_2) until achieving 95% monolayer confluence. Mechanical wounding was performed by creating three parallel linear defects in the cellular monolayer using a sterile 100 μL micropipette tip. Post-incubation for 24 hours under normal growth conditions, cellular migration patterns were quantitatively analyzed through phase-contrast microscopy (Olympus, Japan). The wound closure dynamics were evaluated by measuring inter-scratch distances at predetermined time points, with healing kinetics calculated using ImageJ analysis software.

2.9. Transwell Invasion Assay

Twenty-four hours post-transfection, HepG2 and MHCC97H hepatocellular carcinoma cells were harvested for invasion capacity evaluation using Transwell chambers. Pre-chilled serum-free DMEM was used to prepare a 10% Matrigel solution (BD Biosciences), with 100 μL aliquots applied to upper chamber membranes and allowed to polymerize for 1 hour at 37°C. Following PBS rinsing, cells were resuspended in serum-free medium at 2×10^5 cells/mL density. Each upper compartment received 200 μL cell suspension, while 600 μL complete growth medium was added to lower chambers. After 24-hour incubation, non-migratory cells were mechanically removed from upper surfaces. Invaded cells on membrane undersides were fixed with 4% paraformaldehyde (15 min) and subsequently stained with 0.5% crystal violet solution. Cellular invasion was quantified using an inverted phase-contrast microscope (Olympus BX53) with five randomly selected fields analyzed per membrane.

2.10.Cell Apoptosis Analysis

Following transfection, HepG2 and MHCC97H hepatocellular carcinoma cells were harvested via centrifugation at 800 rpm for 3 minutes. After three washes with ice-cold PBS, cellular apoptosis was evaluated through dual staining with Annexin V-FITC and propidium iodide (ThermoFisher Scientific). Apoptotic cell populations were subsequently quantified on a BD FACSCanto™ II flow cytometer using standardized acquisition protocols.

2.10.1. In Vivo Tumorigenesis Assays

Thirty-five-day-old male BALB/c-nu mice (Charles River Laboratories, Beijing) were maintained under controlled environmental conditions with ad libitum access to food and water. All experimental procedures received ethical approval from the Medical Ethics Committee of Youjiang Medical University for Nationalities (Protocol No. 2022092001). Animals were randomly allocated into two experimental groups (n=7/group): sh-NC control and sh-circ knockdown cohorts. MHCC97H cells (1×10^7) stably expressing sh-circ or control vectors were suspended in 100 μl physiological saline and implanted subcutaneously in the right axillary region. Tumor growth was monitored weekly using caliper measurements. Following 30 days of observation, when significant weight loss occurred, animals were humanely euthanized via pentobarbital sodium administration (120 mg/kg, intraperitoneal injection). Cessation of vital signs (respiratory arrest, motor inactivity, and pupillary dilation) was confirmed prior to tumor resection for subsequent dimensional analysis (length, width) and mass determination.

2.10.2. Western Blot

Following a 48-hour transfection period, HCC cells underwent three PBS rinses with ice-cold solution. Total cellular proteins were extracted using RIPA buffer (Solarbio, China) and quantified through Pierce BCA assay (Beyotime, China). Protein samples (30 μg per lane) underwent electrophoretic separation on 10% SDS-PAGE gels followed by electroblotting onto PVDF membranes (Millipore, USA). Membranes were blocked with 5% non-fat milk in TBST for 2 hours at ambient temperature before overnight incubation at 4°C with primary antibodies: β-actin (1:3000, ab227387) and CELF2 (1:3000, ab179447) from Abcam. Subsequent hybridization with HRP-conjugated secondary antibodies (1:5000, Invitrogen) proceeded for 60 minutes prior to chemiluminescent detection.

2.10.3. Luciferase Reporter Assay

The dual-luciferase reporter plasmids were commercially acquired from GenePharma Co., Ltd (Suzhou, China). The full-length sequences of hsa_circ_0006421 and the CELF2 3'-untranslated region (UTR) containing predicted miR-134-5p binding motifs were cloned into the pmirGLO dual-luciferase reporter vector. HEK293T cells were seeded in 24-well plates and cultured overnight to 70-80% confluence prior to transfection. Cells were subsequently transfected with 1 μg of either WT or MUT reporter plasmids along with 1.5 μL of miR-134-5p mimic/negative control (NC) using Lipofectamine 3000-mediated transfection. Following 48-hour incubation, firefly and Renilla luciferase activities were measured using the Dual-Luciferase Reporter Assay System (Promega) according to manufacturer protocols.

2.10.4. Statistical Analysis

All experiments were conducted in triplicate. Data are presented as mean values ± standard deviation (SD). Statistical analyses were carried out using R software (version 4.0.2). Comparative analysis of hsa_circ_0006421 expression levels between liver cancer tissues and adjacent normal tissues was performed using the Wilcoxon signed-rank test. Parametric comparisons were evaluated through Student's t-test and one-way ANOVA, while categorical variables were assessed with Fisher's exact test. A significance threshold of $p<0.05$ was applied for all statistical tests.

3. Results

3.1. Differential Expression of CircRNAs in HCC

To identify DEcircRNAs in HCC, the limma R software package was used to analyze the circRNA expression profiles from HCC-related datasets GSE97332 and high-throughput sequencing datasets. CircRNAs with thresholds of adj.*P*.Val <0.05 and |logfold change (FC)| >1 were considered DEcircRNAs. A total of 841 and 2449 DEcircRNAs were identified in the GSE97332 and high-throughput sequencing datasets, respectively. Using the pheatmap and Venn diagram packages, 28 overlapping DEcircRNAs were identified in these two datasets (Fig. 1A, 1B, 1C). We found that the biological function of hsa_circ_0006421 in HCC has not yet been reported. Thus, hsa_circ_0006421 was chosen for further experiments.

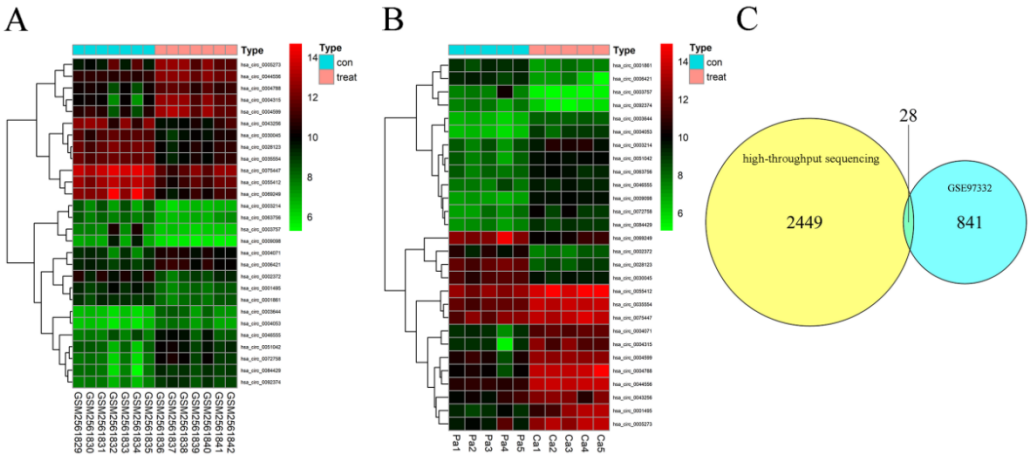

Figure 1. DEcircRNAs in HCC tissues compared with the adjacent tissues. (A) The heatmaps of the DEcircRNA profiles in HCC and compared adjacent tissues in GSE97332 dataset. (B) The heatmaps of the DEcircRNA profiles in HCC and compared adjacent tissues in high-throughput sequencing. (C) Venn diagram of overlapping DEcircRNAs from intersection of GSE97332 and high-throughput sequencing datasets

3.2. Hsa_circ_0006421 is Abnormally Low Expressed in HCC Tissues

Analysis of 34 paired HCC and paracancerous tissues revealed significant downregulation of hsa_circ_0006421 in tumor specimens (22/34 cases, Fig. 2). Clinicopathological analysis demonstrated a significant correlation between hsa_circ_0006421 expression and cirrhosis history (p=0.042, Table 2). These findings suggest hsa_circ_0006421 dysregulation in HCC progression and its potential tumor-suppressive role, particularly in patients with pre-existing cirrhosis.

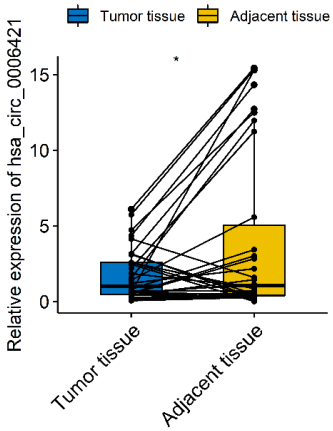

Figure 2. Downregulation of hsa_circ_0006421 is observed in HCC tissues. Comparative analysis revealed differential expression patterns of hsa_circ_0006421 across 34 paired HCC and adjacent normal tissue specimens. *p < 0.05, **p < 0.01 and ***p < 0.001.

Table 2. Hsa_circ_0006421 dysregulation demonstrates significant associations with advanced clinicopathological features in HCC

Characteristics	N=34	Expression of hsa_circ_0006421		*p*
		Low(n=22)	High(n=12)	
Age				0.462
≧50y	13	7	6	
＜50y	21	15	6	
Gender				1.00
Female	5	3	2	
Male	29	19	10	
HBsAg				0.225
Positive	29	20	9	
Negative	5	2	3	
Cirrhosis history				0.042
Positive	29	21	8	
Negative	5	1	4	
Tumor size				0.128
≧5cm	20	15	5	
＜5cm	14	7	7	
AFP				0.315
≧20ng/mL	23	16	7	
＜20ng/mL	11	6	5	
T classification				0.08
T3-T4	21	16	5	
T1-T2	13	6	7	
Tumor number				0.610
≧2	11	7	4	
1	23	15	8	

3.3. Hsa_circ_0006421 Exerts tumor-suppressive Effects in HCC through Significant Inhibition of Malignant Proliferation and Metastatic Potential in Cellular Models.

To investigate hsa_circ_0006421's functional role in HCC, we employed siRNA (si-circ) and lentiviral vectors (sh-circ) to knock down its expression in HepG2 and MHCC97H cells, while constructing an overexpression plasmid (over-circ). qRT-PCR confirmed successful knockdown and overexpression in both cell lines **(Fig. 3A)**. Functional analyses revealed that hsa_circ_0006421 overexpression significantly inhibited viability (**Fig. 3B-C**), migration (**Fig. 3D**), and invasion (**Fig. 3E**) while enhancing apoptotic activity (**Fig. 3F**). Conversely, hsa_circ_0006421 suppression produced opposing cellular effects. These findings demonstrate that hsa_circ_0006421 acts as a tumor suppressor in HCC by regulating multiple malignant phenotypes.

3.4. Hsa_circ_0006421 Inhibits HCC Tumors Growth in Vivo

To investigate hsa_circ_0006421's role in HCC tumorigenesis, we developed a xenograft model using nude mice implanted with MHCC97H cells stably transfected with sh-circ or sh-NC. Subcutaneous tumors formed by day 9, with tumor dimensions monitored weekly. After 30 days, hsa_circ_0006421 knockdown demonstrated significant suppression of tumor progression, showing marked reductions in both volume and mass compared to controls (n=7) **(Fig. 4A-D)**.

3.5. Hsa_circ_0006421 Suppresses HCC Progression by Targeting the miR-134-5p/CELF2 Signaling Axis

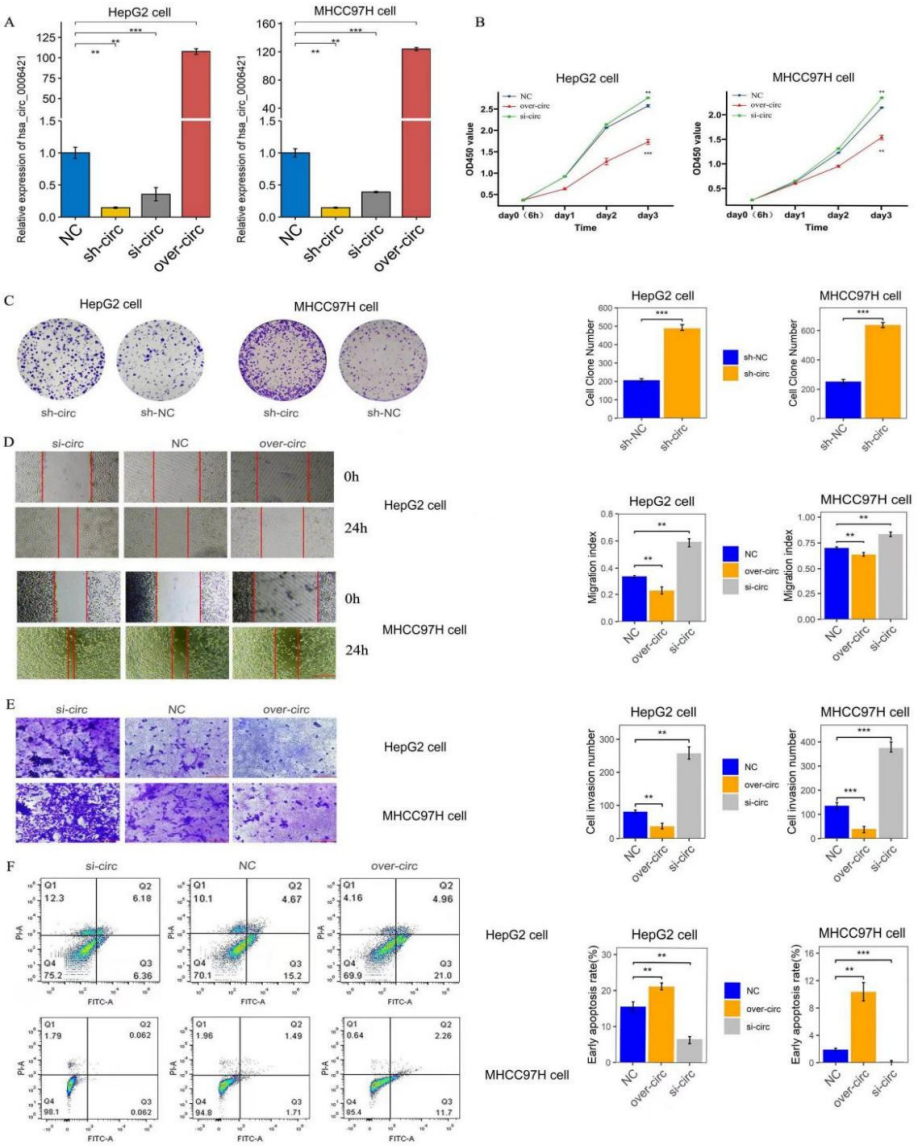

Figure 3. Functional characterization of hsa_circ_0006421 in hepatocellular carcinoma progression. qRT-PCR analysis confirmed successful modulation of hsa_circ_0006421 expression in engineered HCC cell lines (A). Functional analysis revealed that hsa_circ_0006421 knockdown significantly enhanced cellular proliferation, as evidenced by CCK-8 viability assays (B) and colony formation capacity (C). Conversely, hsa_circ_0006421 overexpression exerted tumor-suppressive effects, markedly inhibiting HCC cell migration (D) and invasion potential in transwell assays (E). Flow cytometric analysis with Annexin V/PI dual staining demonstrated that hsa_circ_0006421 depletion attenuated apoptosis, while its ectopic expression promoted programmed cell death (F). All quantitative data represent mean ± SD from triplicate experiments (scale bars = 100 μm).

Recent research has demonstrated that hsa_circ_0006421 exerts tumor-suppressive effects in gastric cancer by modulating the miR-134-5p/CELF2 axis [17]. To explore its potential regulatory mechanism in hepatocellular carcinoma (HCC), we performed hsa_circ_0006421 overexpression in HepG2 and MHCC97H cell lines. Subsequent analysis revealed marked downregulation of miR-134-5p (**Fig. 5A**), suggesting inverse regulatory relationship. Through luciferase reporter assays with constructed wild-type (WT) and mutant (MUT) vectors, we confirmed direct binding between hsa_circ_0006421 and miR-134-5p (**Fig. 5B**). Significant reduction in luciferase activity was observed in HEK293T cells co-transfected with miR-134-5p mimics and WT-hsa_circ_0006421, while MUT-hsa_circ_0006421 maintained stable luminescence (**Fig. 5C**), establishing their functional interaction.

Further investigation of miR-134-5p/CELF2 interplay in HCC demonstrated that miR-134-5p overexpression substantially decreased CELF2 mRNA levels through qRT-PCR analysis (Fig. 5D). Bioinformatics prediction and subsequent experimental validation identified specific binding sites between these molecules (**Fig. 5E**). Dual-luciferase assays confirmed reduced activity in WT CELF2 3'-UTR groups following miR-134-5p mimic transfection, with no alteration in MUT groups (**Fig. 5F**), confirming their direct regulatory relationship.

To elucidate the hsa_circ_0006421/CELF2 regulatory axis, we performed genetic manipulation using siRNA knockdown and plasmid overexpression in HCC cell models. Western blot analysis revealed that hsa_circ_0006421 expression levels directly correlated with CELF2 protein abundance (**Fig. 5G**). These collective findings substantiate our hypothesis that hsa_circ_0006421 impedes HCC progression through miR-134-5p-mediated regulation of CELF2 expression.

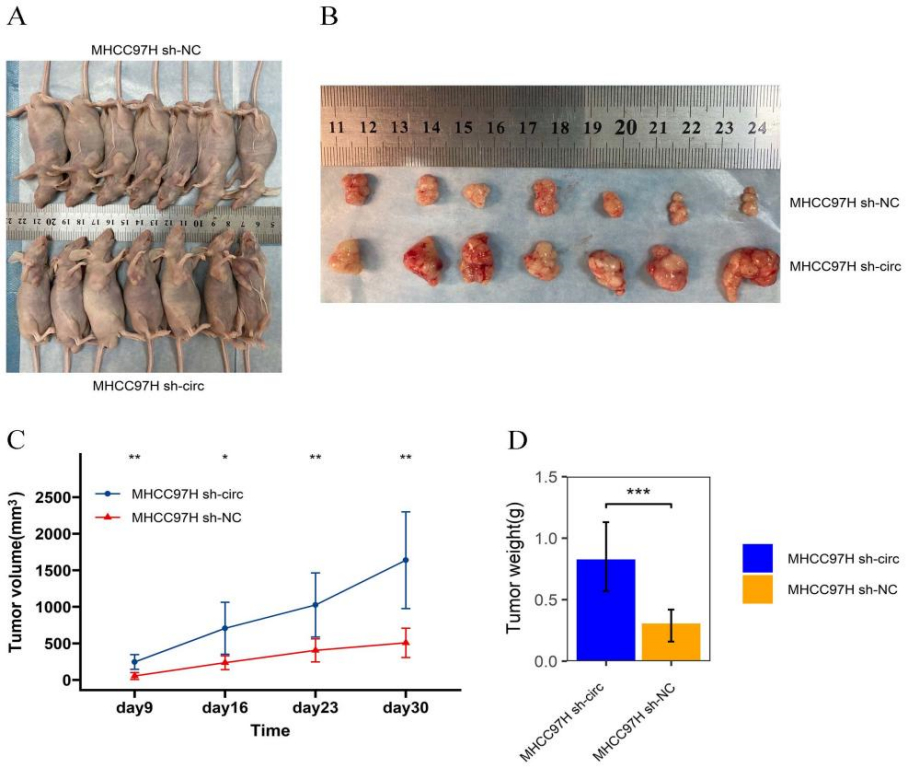

Figure 4. Knockdown of hsa_circ_0006421 promoted tumorigenesis of MHCC97H cells in vivo. (A, B) The xenograft tumor mode showed that tumors grown from the sh-circ group were bigger than those grown from the sh-NC group (n=7). (C, D) Compared with the sh-NC group, the sh-circ group had tumors with significantly increased volume and weight.

4. Discussion

Hepatocellular carcinoma (HCC) has emerged as a globally prevalent refractory malignancy due to its intricate pathogenesis and elevated recurrence rates [18]. The substantial disease burden in China necessitates urgent identification of specific biomarkers and therapeutic strategies for early-stage HCC management to enhance patient survival and clinical outcomes [19]. Hepatocarcinogenesis fundamentally stems from genetic alterations in hepatic cells, leading to dysregulated proliferation-apoptosis homeostasis [20].

Circular RNAs (circRNAs), a subclass of non-coding RNAs, have garnered significant research interest for their multifaceted roles in oncogenesis and tumor progression [21]. Advanced computational biology frameworks coupled with high-resolution sequencing technologies provide actionable insights into gene regulation dynamics, revolutionizing HCC diagnosis through liquid biopsy biomarkers and enabling personalized treatment regimens targeting oncogenic signaling pathways. Mounting clinical studies reveal that circRNA expression aberrations serve as molecular determinants for intractable diseases, particularly therapy-resistant cancers. For instance, hsa_circ_0002232 exhibits tumor-suppressive effects in colorectal cancer through TGF-β/Smad pathway modulation[22]. The circKDM4B/miR-675/NEDD4L axis constitutes a novel therapeutic target for metastatic breast cancer, where circRNA-directed miRNA sponging combined with enhanced proteasomal degradation of malignancy drivers significantly attenuates cancer cell motility and matrix invasion capacity[23]. The circROBO1-KLF5-FUS autoregulatory axis drives breast oncogenesis through coordinated potentiation of transcriptional programs governing hepatic tropism and metastatic niche formation

[24]. CircVAMP3 impedes hepatocellular carcinoma development through translational inhibition of c-Myc[25]. Our investigation identified hsa_circ_0006421 as differentially expressed in HCC through integrated genomic analyses, suggesting its potential regulatory significance in hepatocarcinogenesis. Quantitative reverse transcription-polymerase chain reaction (qRT-PCR) validation confirmed marked hsa_circ_0006421 downregulation in HCC specimens, particularly in cirrhotic patients, indicating its putative tumor-suppressive function.

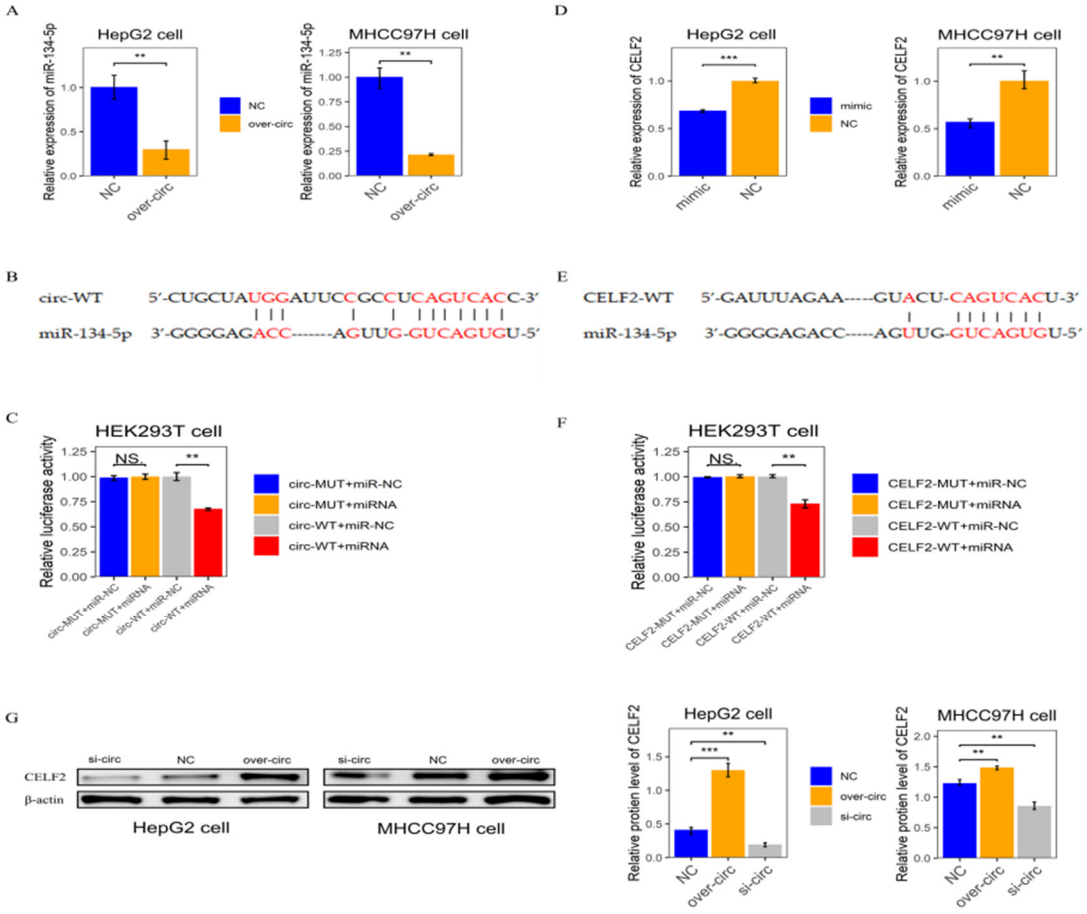

Figure 5. Hsa_circ_0006421 suppresses hepatocellular carcinoma progression through the miR-134-5p/CELF2 regulatory axis. qRT-PCR analysis demonstrated that hsa_circ_0006421 overexpression significantly downregulated miR-134-5p expression in both HepG2 and MHCC97H cell lines(A). Bioinformatics prediction and dual-luciferase reporter assays confirmed direct binding between hsa_circ_0006421 and miR-134-5p, with miR-134-5p mimics specifically reducing wild-type (WT) hsa_circ_0006421 3'UTR luciferase activity(B-C). miR-134-5p exhibited negative regulatory effects on CELF2 expression, as evidenced by qRT-PCR quantification(D). Subsequent dual-luciferase assays identified CELF2 as a direct target of miR-134-5p through binding site verification in the WT CELF2 3'UTR(E-F). Western blot analysis confirmed that hsa_circ_0006421 upregulation enhances CELF2 protein expression in HCC cells, establishing a complete ceRNA regulatory mechanism(G).

Mechanistically, miR-134-5p's oncogenic potential in early LUAD progression may stem from its targeting of tumor suppressor genes, creating a permissive microenvironment for micrometastatic niche formation[26]. Emerging evidence demonstrates that miR-134-5p attenuates acute myeloid leukemia (AML) progression by inhibiting leukemic cell proliferation and malignant potential through modulation of key oncogenic pathways[27].The functional significance and molecular mechanisms of miR-134-5p in hepatocellular carcinoma pathogenesis require rigorous investigation, particularly its regulatory role in tumor microenvironment remodeling and metastatic cascade activation. Our study demonstrates that the tumor-suppressive circular RNA hsa_circ_0006421 functions as a competing endogenous RNA (ceRNA) for miR-134-5p in HCC. qRT-PCR analysis revealed that hsa_circ_0006421 overexpression significantly reduced miR-134-5p levels in HCC cells. Direct interaction was confirmed through dual-luciferase reporter assays. These findings establish miR-134-5p as a key regulatory target of hsa_circ_0006421 in HCC pathogenesis.

After bioinformatic analysis using Starbase v3.0 platform (https://starbase.sysu.edu.cn/index.php). We found that miR-134-5p may have targeted binding with CELF2. As a member of the CUGBP Elav-like family, CELF2 functions as an RNA-binding protein (RBP) [28]. Elevated CELF2 expression correlates with favorable clinical outcomes across multiple malignancies[29]. Experimental evidence demonstrated that CELF2 attenuates breast cancer progression by suppressing NFATc1 expression[30].CELF2 suppresses ovarian cancer cell invasion through stabilization of FAM198B [31]. The oncogenic lncRNA CRNDE promotes HCC by inducing epigenetic downregulation of CELF2 and LATS2 [32]. The STYXL1-PI3K/Akt signaling axis drives HCC cell invasion by transcriptional repression of CELF2[33]. qRT-PCR analysis revealed that miR-134-5p significantly downregulated CELF2 expression in hepatocellular carcinoma (HCC). Dual-luciferase reporter assays further demonstrated decreased luciferase activity in the wild-type CELF2 3'-UTR group following miR-134-5p mimic transfection, confirming their direct targeting interaction. To

investigate hsa_circ_0006421's role in modulating this regulatory axis, we performed gain- and loss-of-function experiments using plasmid overexpression and siRNA-mediated knockdown in HCC-derived HepG2 and MHCC97H cell lines. Western blot analysis showed corresponding dose-dependent changes in CELF2 protein levels, establishing hsa_circ_0006421 as a positive regulator of CELF2 expression through miR-134-5p sequestration.

Our findings indicate that hsa_circ_0006421 functions as a tumor suppressor in HCC pathogenesis, with its reduced expression potentially elevating hepatocarcinogenesis risk in cirrhotic patients. Mechanistically, hsa_circ_0006421 exerts anti-tumor effects by competitively binding miR-134-5p to enhance CELF2 expression, thereby inhibiting malignant progression. This circRNA-mediated regulatory network presents novel therapeutic opportunities for HCC intervention.

5. Conclusion

Collectively, our findings demonstrate that hsa_circ_0006421 suppresses hepatocellular carcinoma progression by functioning as a ceRNA through competitive binding to miR-134-5p to upregulate CELF2, suggesting a potential therapeutic strategy against HCC proliferation.

Ethics Approval and Consent to Participate

The research protocol complied with the Declaration of Helsinki and received dual ethical approvals: from the Institutional Review Board of Affiliated Hospital, Youjiang Medical University for Nationalities (No. YYFY-LL-2022-13) and the University Medical Ethics Committee (No. 2022092001), encompassing both human and animal studies.

Availability of Data and Materials

All research-generated datasets are fully accessible through both primary text documentation and extended digital appendices

Acknowledgments

This study was supported by the Guangxi Science and Technology Project (Grant No. 2018GXNSFAA281187).

References

[1] HUANG X Y, HUANG Z L, ZHANG P B, et al. CircRNA-100338 Is Associated With mTOR Signaling Pathway and Poor Prognosis in Hepatocellular Carcinoma [J]. Front Oncol, 2019, 9: 392.

[2] FERLAY J, COLOMBET M, SOERJOMATARAM I, et al. Cancer statistics for the year 2020: An overview [J]. Int J Cancer, 2021.

[3] SUNG H, FERLAY J, SIEGEL R L, et al. Global Cancer Statistics 2020: GLOBOCAN Estimates of Incidence and Mortality Worldwide for 36 Cancers in 185 Countries [J]. CA Cancer J Clin, 2021, 71(3): 209-249.

[4] HUANG Z, ZHOU J K, PENG Y, et al.The role of long noncoding RNAs in hepatocellular carcinoma [J]. Mol Cancer, 2020, 19(1): 77.

[5] ZHOU H, ZHENG X D, LIN C M, et al. Advancement and properties of circular RNAs in prostate cancer: An emerging and compelling frontier for discovering [J]. Int J Biol Sci, 2021, 17(2): 651-669.

[6] LIU C, LI N, DAI G, et al.A narrative review of circular RNAs as potential biomarkers and therapeutic targets for cardiovascular diseases [J]. Ann Transl Med, 2021, 9(7): 578.

[7] SHEN H, LIU B, XU J, et al. Circular RNAs: characteristics, biogenesis, mechanisms and functions in liver cancer [J]. J Hema-tol Oncol, 2021, 14(1): 134.

[8] SONG T F, XU A L, CHEN X H, et al. Circular RNA circRNA_101996 promoted cervical cancer development by regulating miR-1236-3p/TRIM37 axis[J]. Kaohsiung J Med Sci, 2021, 37(7): 547-561.

[9] ZHENG X, HUANG M, XING L, et al. The circRNA circSEPT9 mediated by E2F1 and EIF4A3 facilitates the carcinogenesis and development of triple-negative breast cancer [J]. Mol Cancer, 2020, 19(1): 73.

[10] LI J, MA M, YANG X, et al. Circular HER2 RNA positive triple negative breast cancer is sensitive to Pertuzumab[J]. Mol Cancer, 2020, 19(1): 142.

[11] XU H, LIU Y, CHENG P, et al. CircRNA_0000392 promotes colorectal cancer progression through the miR-193a-5p/PIK3R3/AKT axis [J]. J Exp Clin Cancer Res, 2020, 39(1): 283.

[12] ZHAO C X, YAN Z X, WEN J J, et al. CircEAF2 counteracts Epstein-Barr virus-positive diffuse large B-cell lymphoma progression via miR-BART19-3p/APC/beta-catenin axis [J]. Mol Cancer, 2021, 20(1): 153.

[13] WANG G, SUN D, LI W, et al. CircRNA_100290 promotes GC cell proliferation and invasion via the miR-29b-3p/ITGA11 axis and is regulated by EIF4A3[J]. Cancer Cell Int, 2021, 21(1): 324.

[14] XU J, JI L, LIANG Y, et al. CircRNA-SORE mediates sorafenib resistance in hepatocellular carcinoma by stabilizing YBX1 [J]. Signal Transduct Target Ther, 2020, 5(1): 298.

[15] CAO P, MA B, SUN D, et al. hsa_circ_0003410 promotes hepatocellular carcinoma progression by increasing the ratio of M2/M1 macrophages through the miR-139-3p/CCL5 axis [J]. Cancer Sci, 2022, 113(2): 634-647.

[16] WU S, YANG J, XU H, et al. Circular RNA circGLIS3 promotes bladder cancer proliferation via the miR-1273f/SKP1/Cyclin D1 axis[J]. Cell Biol Toxicol, 2022, 38(1): 129-146.

[17] FAN H N, ZHAO X Y, LIANG R, et al. CircPTK2 inhibits the tumorigenesis and metastasis of gastric cancer by sponging miR-134-5p and activating CELF2/PTEN signaling [J]. Pathol Res Pract, 2021, 227: 153615.

[18] LIU D, LIU W, CHEN X, et al. circKCNN2 suppresses the recurrence of hepatocellular carcinoma at least partially via regu-lating miR-520c-3p/methyl-DNA-binding domain protein 2 axis [J]. Clin Transl Med, 2022, 12(1): e662.

[19] LUO Z, LU L, TANG Q, et al. CircCAMSAP1 promotes hepatocellular carcinoma progression through miR-1294/GRAMD1A pathway [J]. J Cell Mol Med, 2021, 25(8): 3793-3802.

[20] ZHANG P F, WEI C Y, HUANG X Y, et al. Circular RNA circTRIM33-12 acts as the sponge of MicroRNA-191 to suppress hepatocellular carcinoma progression[J]. Mol Cancer, 2019, 18(1): 105.

[21] WANG Z, LEI X, WU F X. Identifying Cancer-Specific circRNA-RBP Binding Sites Based on Deep Learning[J]. Molecules,2019, 24(22).

[22] ZHENG L, LIANG H, ZHANG Q, et al. circPTEN1, a circular RNA generated from PTEN, suppresses cancer progression through inhibition of TGF-beta/Smad signaling [J]. Mol Cancer, 2022, 21(1): 41.

[23] GUO X Y, LIU T T, ZHU W J, et al. CircKDM4B suppresses breast cancer progression via the miR-675/NEDD4L axis[J]. Onco-gene, 2022.

[24] WANG Z, YANG L, WU P, et al. The circROBO1/KLF5/FUS feedback loop regulates the liver metastasis of breast cancer by inhibiting the selective autophagy of afadin[J]. Mol Cancer, 2022, 21(1): 29.

[25] CHEN S, CAO X, ZHANG J, et al. circVAMP3 Drives CAPRIN1 Phase Separation and Inhibits Hepatocellular Carcinoma by Suppressing c-Myc Translation [J]. Adv Sci (Weinh), 2022: e2103817.

[26] ZHANG L, HUANG P, LI Q, et al. miR-134-5p Promotes Stage I Lung Adenocarcinoma Metastasis and Chemoresistance by Targeting DAB2 [J]. Mol Ther Nucleic Acids, 2019,18: 627-637.

[27] LIU Y, CHEN X, LIU J, et al. Circular RNA circ_0004277 Inhibits Acute Myeloid Leukemia Progression Through MicroRNA-134-5p / Single stranded DNA binding protein 2[J]. Bioengineered, 2022, 13(4): 9662-9673.

[28] LIAO C, CHEN W, WANG J. MicroRNA-20a Regulates Glioma Cell Proliferation, Invasion, and Apoptosis by Targeting CUGBP Elav-Like Family Member 2[J]. World Neurosurg, 2019, 121: e519-e527.

[29] WANG L, LIU Z, LIU L, et al. CELF2 is a candidate prognostic and immunotherapy biomarker in triple-negative breast cancer and lung squamous cell carcinoma: A pan-cancer analysis [J]. J Cell Mol Med, 2021, 25(15): 7559-7574.

[30] ZHOU L, XIE X. RNA-binding protein CELF2 inhibits breast cancer cell invasion and angiogenesis by downregulating NFATc1 [J]. Exp Ther Med, 2021, 22(2): 898.

[31] GUO Q, WU Y, GUO X, et al. The RNA-Binding Protein CELF2 Inhibits Ovarian Cancer Progression by Stabilizing FAM198B [J]. Mol Ther Nucleic Acids, 2021, 23: 169-184.

[32] XIE S C, ZHANG J Q, JIANG X L, et al. LncRNA CRNDE facilitates epigenetic suppression of CELF2 and LATS2 to promote proliferation, migration and chemoresistance in hepatocellular carcinoma[J]. Cell Death Dis, 2020, 11(8): 676.

[33] WU J Z, JIANG N, LIN J M, et al. STYXL1 promotes malignant progression of hepatocellular carcinoma via downregulating CELF2 through the PI3K/Akt pathway [J]. Eur Rev Med Pharmacol Sci, 2020, 24(6): 2977-2985.